Method for Improving Digital Elevation Model Precision of Consumer Level Unmanned Aerial Vehicles

Qiuxin XIA*, Zhong LI, Yong ZHOU, Ensi ZHANG, Gang YANG

Nanjing Les Information Technology Co., Ltd., Nanjing 210001, China

Abstract Currently, the aerial survey system of low-altitude unmanned aerial vehicles (UAVs) has been widely used in acquiring digital map 4D products, mapping, digital linear maps, and other aspects. However, there are problems, such as low precision and weak practicability in constructing digital elevation model (DEM) products through the data collected using consumption level UAVs. Therefore, improving the accuracy of DEM products obtained by consumption level UAVs is a crucial and complex issue in the research of UAV aerial survey systems. In precision elevation measurement, the geodetic height of a certain number of ground points with reasonable distribution in the region is often obtained first. Then, the normal height of the ground points is obtained by leveling, and the elevation residual value surface of the region is fitted. Finally, the normal height of the points to be solved in the region is obtained by fitting the elevation residual surface. Therefore, the elevation residual fitting method was used to improve the accuracy of consumer UAV DEM products in this study. First, a high-quality ground point cloud was obtained by constructing the gradient filtering-cloth simulation filtering (GF-CSF) model. Second, an abnormal elevation fitting residual DEM model was constructed. Lastly, the final DEM was obtained using the DEM difference method. The experimental results show that among the 20 random sampling inspection points, the average elevation residual was 2.3 mm, and the root mean square error (RMSE) was 16.7 mm after the DEM accuracy was improved by the method. The average elevation residual without improving the DEM accuracy was 28.6 mm, and RMSE was 33.7 mm.

Key words UAV aerial survey; GF; CSF; DEM; Surface fitting

DOI 10.19547/j.issn2152 -3940.2024.02.014

As a part of modern digital map 4D products, DEM promotes the rapid development of the geographic information industry. The use of collected terrain data to build high-quality DEMs has attracted the attention of many researchers. Compared with traditional remote sensing technology, UAV photogrammetry can obtain a large amount of point cloud data in a short time and accurately collect the three-dimensional coordinate information of the Earth's surface. This provides data support for building DEM and digital surface model (DSM) products and is an important data source for high-resolution surface modeling[1-3].

Currently, low-altitude UAV aerial survey systems are widely used in the acquisition of digital map 4D products, mapping, digital linear maps, and so on. Improving the accuracy of UAV aerial surveys is key to the application. Therefore, many domestic scholars have analyzed and demonstrated the improvement of UAV aerial survey accuracy from the layout of image control points layout[4-6], image acquisition and correction[7-9], image space encryption[10-11], and so forth, which makes the orthophoto image and three-dimensional model obtained by UAV more beautiful, clear, and widely used, and provides many new ways to improve UAV aerial survey accuracy. The aerial survey plane accuracy of consumption level UAVs is at the centimeter level, but the elevation accuracy is at the decimeter level. Therefore, DEM products produced by consumption level UAVs cannot be put into actual aerial survey production. Hence, how to improve the accuracy of DEM products produced by consumer level UAVs is very important. However, there has been little discussion on the improvement of DEM accuracy obtained by UAV aerial surveys. In a precision elevation survey, to obtain the normal height of the points to be solved in a certain area, the geodetic height of a certain number of reasonably distributed ground points in the area is obtained first; then, the normal height (the distance from the ground point along the plumb line to the quasi-geoid) of the ground points is obtained by leveling and the elevation residual (the difference between the normal height of the ground point and the height of the point obtained by the drone) value surface of the area is fitted; finally, the normal height of the points to be solved in the area is obtained from the fitted elevation residual value surface[12-13]. However, this method has rarely been applied to improve the DEM accuracy obtained by UAVs.

In this paper, a method of fitting the surface with elevation residuals to obtain the normal height and improve the DEM accuracy of consumer UAVs was introduced. First, a gradient cloth filter model was constructed to obtain a high-quality ground point cloud (in the point cloud data of the research area processed by the aerial photos, the points after filtering to remove buildings, vegetation and weeds). Second, the abnormal elevation fitting residual DEM model with Global Navigation Satellite System Real-time kinematic (GNSS RTK) measured elevation as the real value was constructed. Third, the final DEM was generated using the raster calculator tool in Arcmap 10.2 to perform raster calculations on two raster images (DEM difference method) and quadratic pol-

Received: January 12, 2024 Accepted: February 18, 2024

* Corresponding author.

ynomial fitting surface. Finally, the accuracy of this method was verified by comparing it with the original DEM.

1 Theoretical basis

1.1 Gradient filtering (GF) Gradient filtering mainly determines whether to reject or receive a selected point by comparing the high difference between two points[14-15]. The threshold of the height difference between two points is defined as a function of the distance between two points, namely the filtering kernel function of $\Delta h_{\max}(d)$.

When filtering, with a decrease in the distance between two points, the point cloud data points with large elevation values are less likely to belong to ground points. It is supposed that A is the original data set, DEM is the ground point set, and d is the distance between points, the point that satisfies the following filter function is the ground point cloud.

$$DEM = \{\rho_i \in A : h_{\rho_i} - h_{\rho_j} \leqslant \Delta h_{\max}(d(\rho_i, \rho_j))\} \quad (1)$$

For a given point ρ_i, if an adjacent point ρ_j cannot be found to make it satisfy formula (2), ρ_i is classified as a ground point.

$$h_{\rho_i} - h_{\rho_j} > \Delta h_{\max}(d(\rho_i, \rho_j)) \quad (2)$$

1.2 Cloth simulation filtering (CSF) The cloth simulation filtering algorithm is a filtering algorithm based on surface adjustment. It inverts the scanned point cloud and then covers the inverted point cloud with a rigid cloth[16-17]. By analyzing the interaction between the cloth node and the points in the corresponding point cloud, the position of the cloth node can be determined to generate an approximate surface shape. Finally, by comparing the distance between the points in the original point cloud and the generated cloth surface, the ground points can be extracted from the point cloud entity. The inversion process is illustrated in Fig. 1.

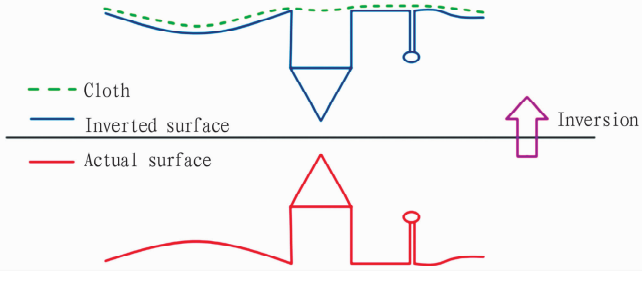

Fig. 1 Schematic diagram of CSF

1.3 Elevation residual fitting The basic idea of the accuracy improvement method in this study was to determine a surface using a group of known elevation residual points in a certain area and then determine the elevation residual values of other measuring points in the area using the surface and points. The determined surface is the best for fitting the data to reflect the changing trend of these discrete data and minimize the sum of squares of error of data points. In the smart3D capture generation model, the elevation difference between the image control point and the corresponding point of the RTK measurement constitutes a functional relationship with its plane coordinates (x, y):

$$\Delta Z = f(x, y) \quad (3)$$

where $f(x, y)$ is a polynomial function. If a quadratic polynomial is taken as an example, the expression is as follows:

$$\Delta Z = a_0 + a_1 x + a_2 y + a_3 xy + a_4 x^2 + a_5 y^2 \quad (4)$$

where a_0, $\cdots$, a_5 are the model parameters to be solved.

Therefore, the least square matrix corresponding to the fitting plane of abnormal elevation based on the polynomial is as follows:

$$\begin{pmatrix} 1, x_1, y_1, x_1y_1, x_1^2, y_1^2 \\ 1, x_2, y_2, x_2y_2, x_2^2, y_2^2 \\ 1, x_3, y_3, x_3y_3, x_3^2, y_3^2 \\ \cdots \\ \cdots \\ 1, x_n, y_n, x_ny_n, x_n^2, y_n^2 \end{pmatrix} \begin{pmatrix} a_0 \\ a_1 \\ a_2 \\ a_3 \\ a_4 \\ a_5 \end{pmatrix} = \begin{pmatrix} \Delta Z_1 \\ \Delta Z_2 \\ \Delta Z_3 \\ \cdots \\ \cdots \\ \Delta Z_n \end{pmatrix} \quad (5)$$

where (x_1, y_1), (x_2, y_2), $\cdots$, (x_n, y_n) are the plane coordinates of the elevation residual points, and ΔZ_1, ΔZ_2, $\cdots$, ΔZ_n are the elevation residual values of the corresponding points. The model parameters can be obtained by applying the solutions of the normal equations to fit the elevation residual values of other points in the survey area.

2 Material and methods

2.1 Study area The experimental area was located in the Shannan campus of Anhui University of Technology, Huainan City, Anhui Province. The experimental area was approximately 0.324 km long and 0.153 km wide, and the survey area was about 0.050 km^2. The experimental area comprised several buildings, neat internal roads, undulating terrain, vegetation, grassland, and water areas. The location of the study area is shown in Fig. 2.

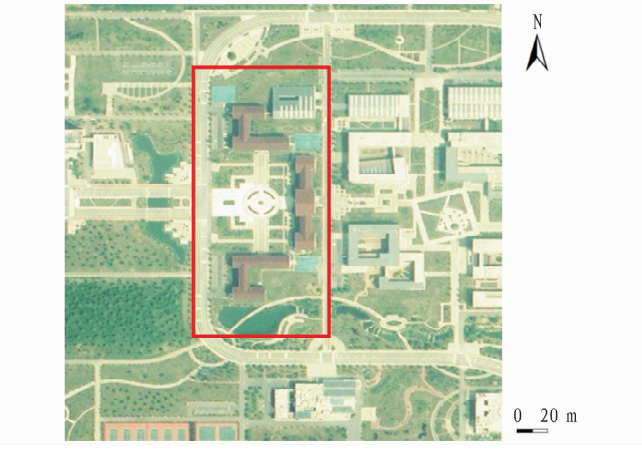

Note: Red rectangle indicates the study area.

Fig. 2 Image of the experimental area

The DJI Phantom 4pro four-rotor UAV was adopted in this study to obtain image data, and its basic parameters are listed in Table 1. The flight altitude of the UAV in the experimental area was 100 m, and the heading and side overlap of the UAV flight was set to 80%.

Before UAV aerial photography, the UAV was used to preliminarily obtain the orthophoto map of the experimental area, determine the terrain and aerial flight route according to the orthophoto map, and preliminarily select the position of the control point. Based on the preselected position, the image control points

were arranged on the ground, and the coordinates of the image control points in the CGCS 2000 coordinate system were collected using RTK. The image control points were arranged by a regional network, and the coordinates were obtained using the GNSS RTK method. RTK was continuously observed four times under the condition of the central fixed solution, and the mean value was taken as the final coordinate. A total of 58 image control points were collected in the study area as control points and checkpoints.

Table 1 UAV-related parameters

UAV model	Phantom 4Pro
Weight-including battery and blades//g	1 390
Image sensor	1 inch CMOS
Maximum horizontal flight speed//km/h	72
Satellite positioning module	GPS/GLONASS dual-mode positioning system
FOV//°	84
Flight time//min	25
Operating ambient temperature//℃	0 – 40

2.2 Construction of GF-CSF model When GF is used to extract ground points in the experimental area, the filtering effect on low vegetation is good, but the filtering effect on tall trees or the top of buildings is poor. Conversely, the filtering effect on the weed beside roads and low vegetation in the area covered by vegetation is poor as CSF is used to extract the ground points in the experimental area, but the filtering effect on buildings and medium and high vegetation is good. To obtain an accurate DEM of the experimental area, a GF-CSF filtering model was constructed by combining GF and CSF in this study. GF was used to obtain the ground seed points firstly, and then CSF was used to filter the ground seed points to ensure that the non-ground point cloud was fully deleted. The specific steps of the filtering method are as follows:

(1) Determining the GF threshold.

(2) Calculating the distance d between the seed point and the adjacent point.

(3) Examining the relationship between d and threshold, and obtain seed ground points.

(4) Initializing the cloth grid, and set C as the virtual grid to the seed ground points.

(5) Projecting all seed ground point data and grid particle data to the same horizontal plane, find each particle of the cloth and the nearest point in the point cloud and record its elevation value.

(6) Calculating the displacement each movable particle in the virtual grid of under the action of gravity and comparing the elevation value of the point with the corresponding point cloud. If the elevation value of a particle is equal to or less than the elevation value of its corresponding point cloud, the particle is placed at the location of the point cloud and set as a non-movable point.

(7) Calculating the displacement of each virtual grid particle under the action of internal force.

(8) Repeating steps 6 and 7. The filtering ends when the maximum elevation change in all virtual particles is sufficiently small or reaches the I set by the user.

(9) Distinguishing between ground and non-ground points. If the distance between the point in the seed ground point and its corresponding virtual particle was less than the filtering threshold, the point was classified as a ground point; otherwise, it was classified as a non-ground point.

In conclusion, the GF-CSF parameter system is $[R, C, I, T]$, where R is the fabric hardness coefficient; C is the fabric grid resolution; I is the maximum number of iterations, and T is the GF-CSF classification threshold.

The flow chart of the ground point cloud acquisition based on the GF-CSF method is shown in Fig. 3.

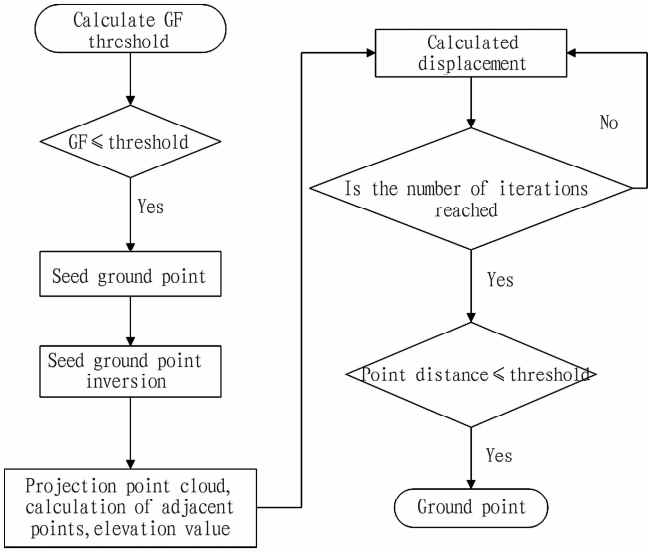

Fig. 3 Flow chart of GF-CSF acquiring ground points

2.3 Elevation fitting method based on polynomial surface model Under the condition of the RTK-centered fixed solution, 50 feature points with the mean value as the orientation of the final coordinate were continuously observed four times. Subsequently, they were selected in an equidistant manner in the experimental area. The experimental area model was generated through smart3D capture high-precision image dense matching technology, and the three-dimensional setting of the feature points under this model was obtained. Thus, the residual value of the feature points in the elevation direction was obtained, and the polynomial fitting plane of each degree was constructed. The evaluation function was constructed through the root mean square error (RMSE) of each polynomial fitting effect and the overall plane fitting effect (R^2), as shown in formula (6).

$$F = \frac{RMSE + (1 - R^2)}{2} \tag{6}$$

The optimal polynomial was then selected to fit the elevation outlier surface according to the lowest point of the evaluation function curve, and the specific steps are as follows:

(1) Obtaining the point coordinates and elevation residual value required by the fitting plane.

(2) Constructing polynomial functions.

(3) Obtaining the model parameters according to the feature

points.

(4) Calculating the *RMSE* and R^2 values under the polynomial fitting of each degree.

(5) Calculating the evaluation function value F, and selecting the optimal degree polynomial according to F.

(6) Determining the fitting plane and obtain the fitting DEM.

In this study, the polynomial degree was selected as primary, secondary, tertiary, and quartic for comparative analysis, and the effects of polynomial fitting feature points were compared. The results are presented in Table 2 and Fig. 4.

Table 2 Polynomial fitting effect

Frequency	*RMSE*//m	R^2	*F*
1	0.03	0.177 8	0.423 7
2	0.01	0.745 6	0.134 5
3	0.02	0.455 1	0.283 6
4	0.03	0.129 6	0.450 3

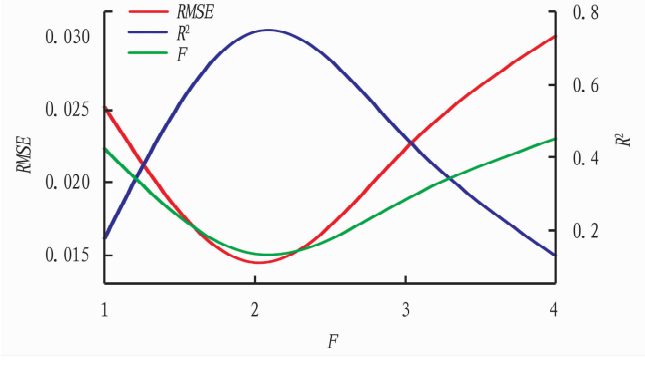

Fig. 4 Polynomial fitting effect

From Table 2, it can be noted that in terms of *RMSE*, when fitting the plane with polynomials of various degrees, the primary, tertiary and quaternary *RMSE* values exceed 0.02, and the secondary *RMSE* value is 0.01. In terms of the overall goodness of fit of the regression equation, the primary, tertiary, and quaternary R^2 are lower than 0.5, and the secondary R^2 value is 0.745 6. As can be observed from Fig. 4, the change trend of the F curve shows that the curve exhibits the "arc distribution" trend, and there is an inflection point during the second time. It can be noted that the quadratic polynomial fitting elevation residual surface has high accuracy.

3 Results

3.1 Data analysis results Smart3D capture professional UAV remote sensing image processing software was used to preliminarily process the aerial photos obtained in the experimental area to minimize the impact of the RTK measuring point error on the final model accuracy. The coordinates of the 58 image control points were measured in the obtained digital orthophoto map, digital surface model, and three-dimensional model of the study area. Further, the gross error was processed using the 3sigma criterion[18], as shown in formula (7).

$$|x_i - \bar{x}| > 3\sqrt{\frac{(x_1-\bar{x})^2 + (x_2-\bar{x})^2 + \cdots + (x_n-\bar{x})^2}{n-1}} \quad (7)$$

where x_i is the elevation difference between the image control point in the generation model and the corresponding point of the RTK measurement; $\bar{x}$ is the mean value of the elevation difference, and n is the number of image control points.

The absolute error value of each sampling point was calculated and compared with three times the standard deviation. If it was greater than three times the standard deviation, it was eliminated, and the steps were repeated until there was no elimination. The smart3D capture high-precision image dense matching technology was used to process the remaining image control points and automatically match the points with the same names in all collected image data. Accurate terrain and feature information was obtained, and dense point clouds were generated. The data processing results are shown in Fig. 5.

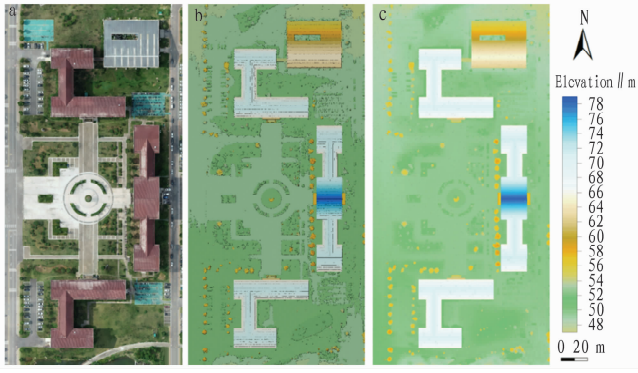

Note: a. DOM; b. DSM render; c. Point cloud.

Fig. 5 Data processing results

3.2 High-precision DEM results By combining the ground point coordinates and elevation outliers obtained in the data acquisition and processing stage, an elevation residual fitting plane based on a quadratic polynomial was constructed. The calculated model parameters are as follows: $a_0 = 1.716e+07$, $a_1 = -2.406$, $a_2 = -9.187$, $a_3 = -6.97e-07$, $a_4 = 4.908e-06$, and $a_5 = 1.323e-06$. The results of the model construction are shown in Fig. 6 (the Y coordinate is translated to a certain extent).

First, the ground point cloud obtained by GF-CSF was used to construct the seed DEM. Second, the surface fitted by a quadratic polynomial was used to construct the residual DEM. Lastly, the final DEM was obtained using the DEM difference method. The results are presented in Fig. 7.

It can be observed from Fig. 7 that the overall elevation trend of the experimental area is the same before and after the accuracy improvement. To verify the effectiveness of DEM accuracy improvement, 20 inspection points were selected in the experimental area based on the principle of the random sampling method. The distribution of sampling points is shown in Fig. 8. The coordinates of inspection points were obtained using the same method as in the data acquisition stage. Then, the elevation of each checkpoint measured using DEM was compared before and after the accuracy improvement, and the elevation residual ΔZ was calculated. The results are presented in Table 3.

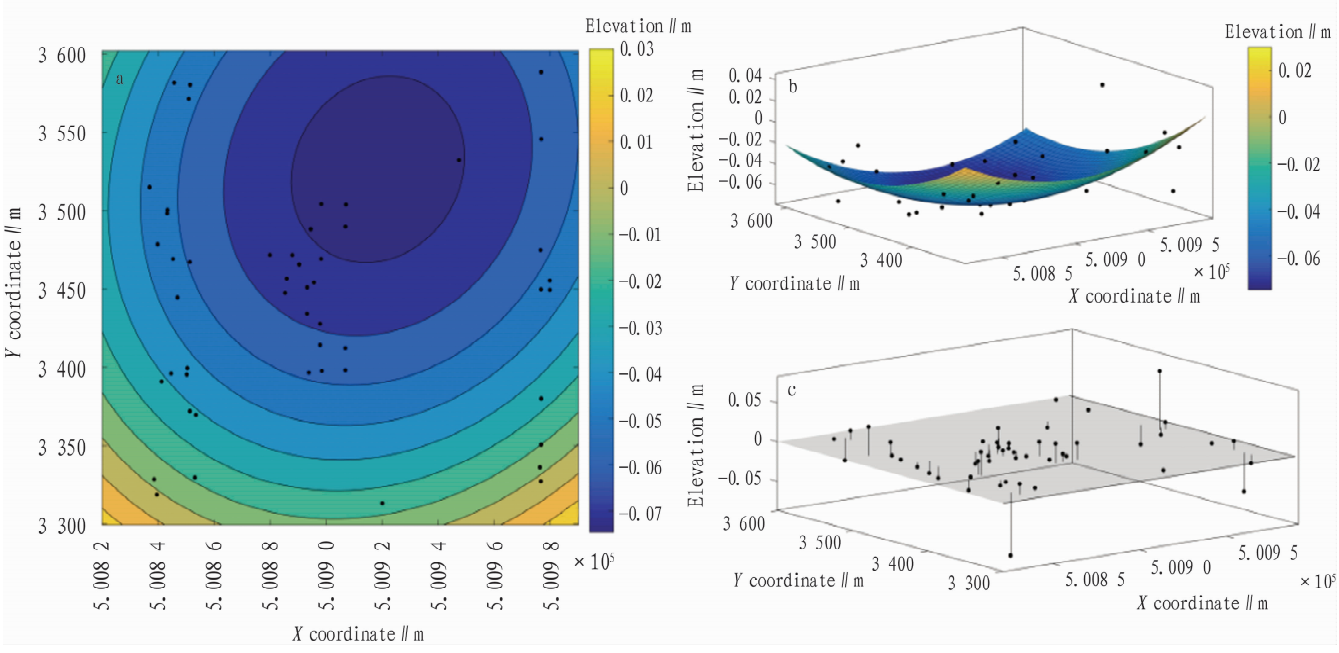

Note: a. Isoline of point distribution; b. Fitting surface; c. Point residual.

Fig. 6 Fitting effect of the experimental area

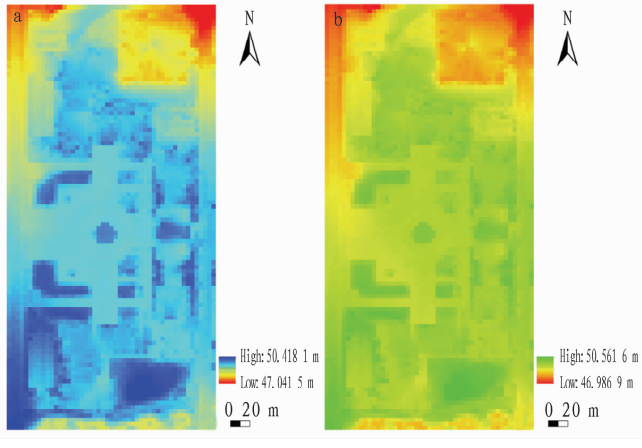

Note: a. Seed DEM; b. Final DEM.

Fig. 7 DEM rendering

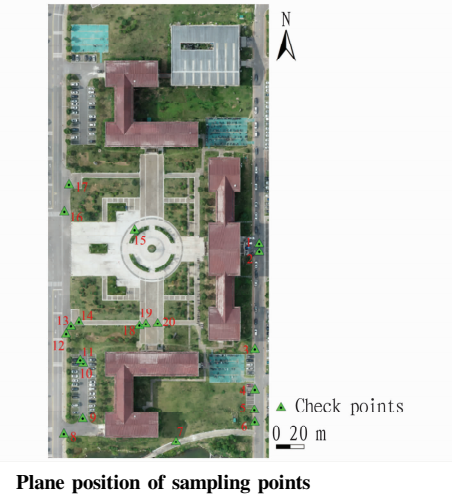

Fig. 8 Plane position of sampling points

Table 3 Sampling inspection results for accuracy improvement effect m

Serial number	GNSS RTK measurement results Z	Before precision improvement		After precision improvement	
		Z	ΔZ	Z	ΔZ
1	49.568 5	49.604 6	−0.036 2	49.559 7	0.008 7
2	49.510 1	49.565 6	−0.055 6	49.519 3	−0.009 3
3	49.388 6	49.427 4	−0.038 9	49.360 3	0.028 2
4	49.509 6	49.533 1	−0.023 6	49.509 5	0
5	49.439 5	49.438 6	0.000 9	49.428 8	0.010 7
6	49.249 0	49.301 0	−0.052 0	49.298 6	−0.049 6
7	49.042 5	49.051 4	−0.008 9	49.054 0	−0.011 5
8	49.705 4	49.716 2	−0.010 9	49.702 0	0.003 3
9	50.110 6	50.096 1	0.014 5	50.097 7	0.012 9
10	49.046 3	49.087 8	−0.041 5	49.043 8	0.002 5
11	49.534 5	49.545 9	−0.011 4	49.534 5	0
12	49.890 2	49.921 5	−0.031 3	49.893 0	−0.002 8
13	49.909 0	49.944 5	−0.035 6	49.916 3	−0.007 4
14	49.888 6	49.931 7	−0.043 1	49.903 3	−0.014 7
15	49.646 7	49.678 9	−0.032 2	49.646 7	0
16	48.867 9	48.914 0	−0.046 1	48.866 6	0.001 3
17	49.636 7	49.656 1	−0.019 4	49.619 5	0.017 2
18	49.442 7	49.469 5	−0.026 9	49.417 9	0.024 7
19	49.413 4	49.456 0	−0.042 6	49.403 5	0.009 9
20	49.405 1	49.437 9	−0.032 8	49.384 7	0.020 4

As shown in Table 3 and Fig. 9, among the 20 randomly sampled inspection points, the DEM was closer to the measured elevation after the accuracy was improved, and the elevation residual was significantly reduced compared with that before the improvement. To further understand the accuracy improvement effect, the RMSE values of the elevation residuals were calculated using the above data. The RMSEs before and after lifting were 33.7 mm and

16.7 mm, respectively, and the DEM accuracy was improved. This method can effectively solve the inaccuracy problem of the aerial survey DEM of low-precision UAVs.

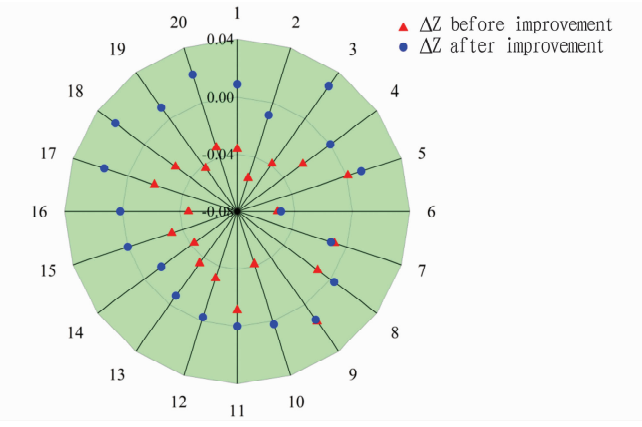

Fig. 9 Sampling inspection of accuracy improvement effect

4 Discussion

The setting of various parameters in the GF-CSF parameter system had a direct impact on the filtering effect. Based on experience and by combining with the topographic characteristics of the experimental area, $[R, C, I, T]$ was set as $[2, 0.6, 500, 0.4]$.

(1) Visual qualitative evaluation. According to the visual qualitative evaluation criteria, it can be determined whether the filtered ground point data meets the mapping requirements. As can be seen from Fig. 10, generally, buildings and trees can be well divided into non-ground points; however, low weeds in some roads cannot be effectively eliminated. Therefore, the overall filtering effect of the edge of the test area must be improved. The vertices of houses close to the scarp are wrongly divided into ground points, while some higher houses are easily wrongly eliminated because dense point cloud data have a high probability of misjudgment in the matching process. Therefore, during post-processing, the dense point cloud data should be thinned, followed by point cloud matching to effectively reduce the misjudgment of point cloud matching at some locations.

(2) Quantitative statistical evaluation. In 2003, the International Society for Photogrammetry and Remote Sensing (ISPRS) proposed an error evaluation standard for filtering algorithm results. In this standard, the filtering result errors are divided into three categories: omission error I refers to the percentage of the number of ground points wrongly divided into non-ground points in the total number of ground points; commission error II is the percentage of the number of ground points wrongly divided among non-ground points in the total number of non-ground points; total error III is the percentage of the total number of ground points and non-ground points incorrectly divided by the total number of point clouds[19-20].

$$I = a/(a+c) \tag{8}$$

$$II = b/(b+d) \tag{9}$$

$$III = (a+b)/(a+b+c+d) \tag{10}$$

where a is the number of ground points wrongly divided into non-ground points; c is the number of ground points correctly divided; b is the number of non-ground points wrongly divided into ground points; d is the number of non-ground points correctly divided. Based on a statistical quantitative method, the effect of point cloud filtering more intuitively reflects the filtering effect of each filtering algorithm. The results of filtering effects are presented in Table 4.

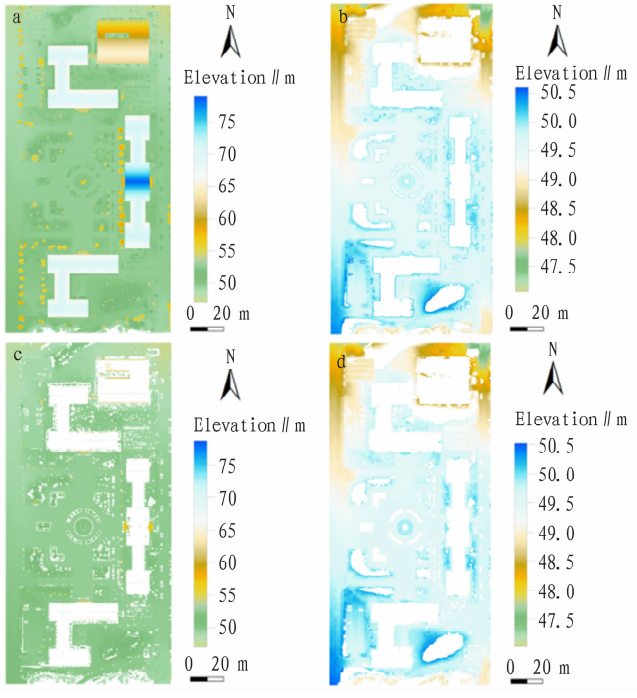

Note: a. Original points cloud; b. CSF ground points; c. GF ground points; d. GF-CSF ground points.

Fig. 10 Comparison of filtering effect

Table 4 Error analysis of filtering results of each filtering algorithm

Types	Reference data		Filtering results		Misjudgment results		Errors // %		
	Ground point	Non-ground point	Ground point	Non-ground point	Ground point	Non-ground point	Omission error	Commission error	Total error
GF	850 533	587 815	573 604	567 577	20 238	276 929	3	33	21
CSF	604 203	834 145	522 904	735 829	98 316	81 299	16	10	12
GF-CSF	650 368	787 980	627 058	709 845	78 135	23 310	11	3	7

Some ground points in the ground covered by higher vegetation were mistakenly classified as non-ground points, while others appeared in the surrounding points of buildings. Commission errors mainly occurred in the low vegetation point cloud that was misclassified as ground points. Table 4 shows that the omission error of the GF in the experiment was 3%, and the commission error was 33%. The omission error of the CSF in the experiment was 16%, and the commission error was 10%. The GF has a good fil-

tering effect on the surrounding low vegetation when filtering non-ground point clouds, but it is not good for the upper point clouds of higher buildings. The CSF had a poor filtering effect for low vegetation, but it had a good filtering effect for high building point clouds. Therefore, the omission error was 11%, the commission error was 3%, and the total error was 7%. The point cloud filtering effect in the entire experimental area was good.

5 Conclusions

(1) The omission error of the GF-CSF method was 11%, the commission error was 3%, and the total error was 7%. The filtering effect of the point cloud in the whole experimental area was good. Therefore, the GF-CSF method had a good filtering effect for areas with most buildings, complex internal roads, undulating terrain, low, medium, and high vegetation, grassland, and water areas.

(2) The fitting results of elevation residuals were not improved with the increase in polynomial order. Compared with the fitting results of first-order and third-order, the fitting accuracy of the second-order polynomial was higher. In this study, the quadratic polynomial was used to fit the DEM. The RMSEs before and after fitting were 33.7 and 16.7 mm, respectively, and the DEM accuracy was improved.

(3) After the GF-CSF has obtained high-quality ground points and constructed DEM, combining the fitting plane method with abnormal elevation values significantly improved the DEM accuracy of low-precision UAVs. However, taking the measured RTK data as the real values, the improved DEM accuracy was only close to the RTK accuracy.

References

[1] GAO X, LIU Y, LI T, *et al.* High precision DEM generation algorithm based on InSAR multi-look iteration[J]. Remote Sensing, 2017, 9(7): 741.

[2] WAEGEMAN W, COTTYN J, WYNS B, *et al.* Classifying carpets based on laser scanner data[J]. Engineering Applications of Artificial Intelligence, 2007, 21(6): 907 – 918.

[3] SERIFOGLU YC, GUNGOR O. Comparison of the performances of ground filtering algorithms and DTM generation from a UAV-based point cloud[J]. Geocarto International, 2016, 33(5): 522 – 53.

[4] ZHAOHUI W, HAO WU, JIANG M. Research and accuracy analysis of image control point arrangement schemes for UAV oblique photography [J]. Bulletin of Surveying and Mapping, 2021(5): 102.

[5] LI C, ZHANG G, LEI T, *et al.* Quick image-processing method of UAV without control points data in earthquake disaster area[J]. Transactions of Nonferrous Metals Society of China, 2011, 21: s523 – s528.

[6] SHAO R, DU C, CHEN H, *et al.* Fast anchor point matching for emergency uav image stitching using position and pose information[J]. Sensors, 2020, 20(7): 2007 – 2007.

[7] SIEKAЙSKI P, PAŠKO S, MALOWANY K, *et al.* Online correction of the mutual miscalibration of multimodal VIS – IR sensors and 3D data on a UAV platform for surveillance applications[J]. Remote Sensing, 2019, 11(21): 2469 – 2469.

[8] GELMAN N, SILAVI A, ANAZODO U. A hybrid strategy for correcting geometric distortion in echo-planar images[J]. Magnetic Resonance Imaging, 2014, 32(5): 590 – 593.

[9] HONKAVAARA E, HAKALA T, MARKELIN L, *et al.* A process for radiometric correction of UAV image blocks[J]. PFG Photogrammetrie, Fernerkundung, Geoinformation, 2012(2): 115 – 127.

[10] CHEN W. Optical multiple-image encryption using three-dimensional space[J]. IEEE Photonics Journal, 2016, 8(2): 1 – 8.

[11] CHEN W, CHEN XA. Space-based optical image encryption[J]. Optics Express, 2010, 18(26): 27095 – 27104.

[12] WANG J, XIE D. GPS elevation fitting study based on ternary polynomial regression[J]. Earth Sciences Research Journal, 2020, 24(2): 201 – 205.

[13] HAICHENG Z, XIDONG M, ZHEN W, *et al.* Optimization of earth gravity field model and its application in elevation fitting[J]. IOP Conference Series: Earth and Environmental Science, 2021, 638(1): 012048.

[14] LI Y, WANG J, LI B, *et al.* An adaptive filtering algorithm of multilevel resolution point cloud[J]. Survey Review, 2020, 53(379): 1 – 12.

[15] KIM MK, KIM S, SOHN HG, *et al.* A new recursive filtering method of terrestrial laser scanning data to preserve ground surface information in steep-slope areas[J]. ISPRS International Journal of Geo-Information, 2017, 6(11): 359.

[16] CAI S, ZHANG W, QI J, *et al.* Applicability analysis of cloth simulation filtering algorithm for mobile LiDAR point cloud[J]. ISPRS-International Archives of the Photogrammetry, Remote Sensing and Spatial Information Sciences, 2018, XLII-3: 107 – 111.

[17] YANG A, WU Z, YANG F, *et al.* Filtering of airborne LiDAR bathymetry based on bidirectional cloth simulation[J]. ISPRS Journal of Photogrammetry and Remote Sensing, 2020, 163: 49 – 61.

[18] PENG DS. Research on ground filtering method of complex terrain in 3D laser point cloud[D]. Qingdao: Shandong University of Science and Technology, 2020.

[19] HAN XF, JIN JS, WANG MJ, *et al.* Guided 3D point cloud filtering [J]. Multimedia Tools and Applications, 2018, 77(13): 17397 – 17411.

[20] ŠTRONER M, URBAN R, REINDL T, *et al.* Evaluation of the georeferencing accuracy of a photogrammetric model using a quadrocopter with onboard GNSS RTK[J]. Sensors, 2020, 20(8): 2318 – 2318.

Copyright Authorization Statement

Should the article be accepted and published by *Meteorological and Environmental Research*, the author hereby grants exclusively to the editorial department of *Meteorological and Environmental Research* the digital reproduction, distribution, compilation and information network transmission rights.